Improved Two-Temperature Model and Its Application in Ultrashort Laser Heating of Metal Films

Lan Jiang

Hai-Lung Tsai[1]

Laser-Based Manufacturing Laboratory,
Department of Mechanical and Aerospace Engineering,
University of Missouri-Rolla,
Rolla, MO 65409

The two-temperature model has been widely used to predict the electron and phonon temperature distributions in ultrashort laser processing of metals. However, estimations of some important thermal and optical properties in the existing two-temperature model are limited to low laser fluences in which the electron temperatures are much lower than the Fermi temperature. This paper extends the existing two-temperature model to high electron temperatures by using full-run quantum treatments to calculate the significantly varying properties, including the electron heat capacity, electron relaxation time, electron conductivity, reflectivity, and absorption coefficient. The proposed model predicts the damage thresholds more accurately than the existing model for gold films when compared with published experimental results. [DOI: 10.1115/1.2035113]

Keywords: Ultrashort Laser, Quantum Mechanics, Metal Thin Film, Two-Temperature Model

1 Introduction

In the past two decades, the ultrashort (typically <10 ps) laser heating of metals and its nonequilibrium energy transport have been very active research topics [1–12]. Nonequilibrium between electrons and phonons is already significant on the picoscecond time order, in which the electron temperature can be much higher than that of the lattice [1,5,7]. The energy transport process in ultrafast laser heating of thin films consists of two stages [1,5–9]. The first stage is the absorption of the laser energy through photon-electron interactions within the ultrashort pulse duration. It takes a few femtoseconds for electrons to reestablish the Fermi distribution. This characteristic time scale, the mean time for electrons to restore their states, is called the electron relaxation time. In spite of nonequilibrium states of the electrons within this characteristic time, the temperature of the electrons is still numerically valid in the limit when the pulse duration is much longer than the electron relaxation time, which is proved by a model using the full Boltzmann transport theory [1]. Within the duration of a single ultrashort pulse, the change of lattice temperature is generally negligible.

The second stage is the energy distribution to the lattice through electron-phonon interactions, typically on the order of tens of picoseconds. Although the electron-phonon collision time may be comparable to the electron-electron collision time, it takes much longer to transfer energy from free electrons to phonons, because the phonon mass is much greater than the electron mass. The characteristic time for the free electrons and the lattice to reach thermal equilibrium is called the thermalization time. In this process, a phonon temperature is used to characterize the Bose distribution.

This two-temperature concept described above was validated by many experiments [3,7,10–14]. Accordingly, the two-temperature model is widely used for the ultrashort laser processing of metals [5–9,15,16]. Especially, Qiu and Tien [5–7] and Qiu et al. [8] group has made excellent theoretical and experimental contributions in this area. However, in the existing two-temperature model, the estimations of the following important properties are limited to temperatures that are much lower than the Fermi temperature T_F that is measured to be 5.9×10^4K for gold [5–8]

- Electron heat capacity $C_e=\gamma T_e$ [7] where T_e is the electron temperature and γ is the electron heat capacity constant. This estimation is limited to $0<T_e<0.1\ T_F$ [17].
- Electron relaxation time $\tau_e=3m_e/(\pi^2 n_e k_B^2 T_e)/k(T_e)$ where m_e is the nonrelativistic mass of a free electron; n_e is the density of the free electron, which is 5.9×10^{22} cm^{-3} for gold; and k_B is the Boltzmann constant [7]. This estimation is based on $C_e=\gamma T_e$ and therefore limited to $0<T_e<0.1\ T_F$ [5,17,18].
- Electron heat conductivity $k_e=(T_e/T_l)k_{\mathrm{eq}}(T_l)$ where k_{eq} is the electron heat conductivity when the electrons and phonons are in thermal equilibrium; and T_l is the lattice temperature [7]. This estimation can be derived and is limited to $T_D<T_e<0.1\ T_F$ where T_D is the Debye temperature of the phonon [17].
- Reflectivity $\Delta T_e/(\Delta T_e)_{\max}\cong\Delta R/(\Delta R)_{\max}$ [8] where R is the reflectivity. This estimation is limited to $300\ \mathrm{K}<T_e<700\ \mathrm{K}$ [8]. Further, $(\Delta T_e)_{\max}$ and $(\Delta R)_{\max}$ are unknown before the estimation.

The aforementioned estimations are limited to low temperatures relative to the Fermi temperature [17]. However, at a fluence near or above the threshold fluence, the electron temperature in metals heated by an ultrashort laser pulse can be comparable to the Fermi temperature. Hence, the two-temperature model is suitable only for low fluences and cannot be used to correctly predict the damage threshold in which the electron temperatures are much higher than $0.1\ T_F$.

This paper extends the existing estimations of optical and thermal properties to high electron temperatures by the following improvements: (1) using the Fermi distribution, the heat capacity of free electrons is calculated; (2) the free electron relaxation time and electron conductivity are determined by using a quantum model derived from the Boltzmann transport equation for dense

[1]Corresponding author; e-mail address: tsai@umr.edu

Contributed by the Heat Transfer Division of ASME for publication in the JOURNAL OF HEAT TRANSFER. Manuscript received: September 21, 2004; final manuscript received: June 7, 2005. Review conducted by: C. P. Grigoropoulos.

plasma; and (3) the free electron heating and interband transition are both taken into account using a modified Drude model with quantum adjustments to calculate the reflectivity and the absorption coefficient. The proposed two-temperature model is employed to calculate the heating process of thin gold films until melting occurs, which is assumed to be the initiation of damage. The predicted damage threshold fluences for 200 nm gold film using the proposed model are in good agreement with published experimental data. The damage threshold fluence as a function of pulse duration is also studied.

2 Theory

2.1 Two-Temperature Model. This paper considers the laser pulse duration in 140 fs–100 ps that are much longer than the electron relaxation time (a few femtoseconds). Hence, the electron temperature, characterized by the Fermi distribution, can be employed [1]. In this study, the laser beam diameter (tens to hundreds of micrometers) is much greater than the optical penetration depth (tens to hundreds of nanometers) and electron penetration depth (tens to hundreds of nanometers) in the nanoscale-thickness thin films and, hence, a one-dimensional model is accurate enough to describe the physical phenomena. The two-temperature model is given below

$$C_e(T_e)\frac{\partial T_e}{\partial t} = \nabla[k_e(T_e)\,\nabla\,T_e] - G(T_e - T_l) + S(z,t) \tag{1}$$

$$C_l(T_l)\frac{\partial T_l}{\partial t} = G(T_e - T_l) \tag{2}$$

where S represents the laser source term, C_l is the lattice heat capacity, and G is the electron-lattice coupling factor estimated by [5]

$$G = \frac{\pi^2 m_e n_e c_s^2}{6\tau(T_e)T_e} \tag{3}$$

where c_s is the speed of sound in bulk material calculated by

$$c_s = \sqrt{\frac{B}{\rho_m}} \tag{4}$$

where B is the bulk modulus and ρ_m is the density.

2.2 Free Electron Heat Capacity. In a wide range of electron temperatures, the full-run quantum treatment should be used to calculate the free electron heat capacity. The average number of electrons $\langle n_k\rangle$ in energy state ε_k obeys the following Fermi distribution:

$$\langle n_k\rangle = \frac{1}{e^{\beta(T_e)[\varepsilon_k - \mu(T_e)]} + 1} \tag{5}$$

where $\beta(T_e) = 1/k_B T_e(t,z)$ and μ is the chemical potential. For free electron gas, the chemical potential can be calculated by [17]

$$\mu(n_e,T_e) = \varepsilon_F(n_e)\left[1 - \frac{\pi^2}{12}\left(\frac{k_B T_e(t,z)}{\varepsilon_F(n_e)}\right)^2 + \frac{\pi^2}{80}\left(\frac{k_B T_e(t,z)}{\varepsilon_F(n_e)}\right)^4\right] \tag{6}$$

where the higher order terms are neglected, z is the depth from the thin film surface, and ε_F is the Fermi energy. Strictly speaking, Eq. (6) is valid for free electrons in equilibrium states only. The free electrons could be disturbed from the Fermi-Dirac distribution by a femtosecond laser pulse. However, when the pulse duration is much longer than the free electron relaxation time, Eq. (6) is still a good approximation, which is similar to the treatment for the electron temperature in this condition [1]. The Fermi energy is determined by [17]

$$\varepsilon_F = \left(\frac{(hc)^2}{8m_e c^2}\right)\left(\frac{3}{\pi}\right)^{2/3} n_e^{2/3} \tag{7}$$

where c is the speed of light in vacuum. The average kinetic energy per electron in J, $\langle\varepsilon\rangle$, is calculated by

$$\langle\varepsilon\rangle = \frac{\sum_k \langle n_k\rangle\varepsilon_k}{N_e} = \frac{\int_0^\infty \frac{1}{e^{\beta(T_e)[\varepsilon-\mu(T_e)]}+1}\rho(\varepsilon)\varepsilon d\varepsilon}{\int_0^\infty \frac{1}{e^{\beta(T_e)[\varepsilon-\mu(T_e)]}+1}\rho(\varepsilon)d\varepsilon} \tag{8}$$

where ε is the kinetic energy of a free electron, N_e is the total number of free electrons, and $\rho(\varepsilon)$ is the density of states given by

$$\rho(\varepsilon) = \frac{8\sqrt{2}\pi m_e^{3/2}}{h^3}\sqrt{\varepsilon} \tag{9}$$

where h is the Planck constant. The heat capacity can be determined by

$$C_e(T_e) = n_e\left(\frac{\partial\langle\varepsilon\rangle}{\partial T_e}\right)_V \tag{10}$$

where V is the volume. In $0 < T_e < 0.1\ T_F$, Eqs. (5)–(10) can be simplified to the following expression [17]:

$$C_e(T_e) = \frac{\pi^2 n_e}{2}\left(\frac{k_B T_e}{\varepsilon_F}\right)k_B \equiv \gamma T_e \tag{11}$$

where γ is the electron heat capacity constant. Equation (11) has been widely employed in the two-temperature model [5–9]. For comparison purpose, the average kinetic energy and specific heat of an ideal electron gas are given below

$$\langle\varepsilon\rangle = \frac{3}{2}k_B T_e, \quad C_e = \frac{3}{2}n_e k_B \tag{12}$$

2.3 Free Electron Heat Conductivity and Relaxation Time. The free electron heat conductivity is expressed by the following Drude theory of metals [17]:

$$k_e(T_e) = \frac{1}{3}\nu_e^2(T_e)\tau_e(T_e)C_e(T_e) \tag{13}$$

where ν_e^2 is the mean square of electron speed. In this study, ν_e^2 and C_e are determined directly by the Fermi distribution based on Eqs. (5)–(10). In Eq. (13), the scattering effects are indirectly considered through the calculation of the free electron relaxation time. In $T_D < T_e < 0.1\ T_F$ and using the values of ν_e^2 and C_e for an ideal gas, Eq. (13) can be simplified to $\tau_e = 3m_e/(\pi^2 n_e k_B^2 T_e)k(T_e)$ [17] that is used in Ref. [7].

In this study, by considering metals as dense plasma [1,17,19,21–23], the free electron relaxation time is calculated as follows by a quantum treatment derived from the Boltzmann transport equation [20,21]:

$$\tau_e(t,z) = \frac{3\sqrt{m_e}(k_B T_e(t,z))^{3/2}}{2\sqrt{2}\pi(Z^*)^2 n_e e^4 \ln\Lambda}\{1 + \exp[-\mu(T_e)/k_B T_e(t,z)]\}F_{1/2} \tag{14}$$

where e is the electron charge, Z^* is the ionization state and is one for gold, $F_{1/2}$ is the Fermi integral, and $\ln\Lambda$ is the Coulomb logarithm determined by

$$\ln\Lambda = \frac{1}{2}\ln\left[1 + \left(\frac{b_{\max}}{b_{\min}}\right)^2\right] \tag{15}$$

where the maximum ($b_{\max}$) and minimum ($b_{\min}$) collision parameters are given by

$$b_{\max}=\frac{(k_BT/m_e)^{1/2}}{\max(\omega,\omega_p)},\quad b_{\min}=\max\left(\frac{Z^*e^2}{k_BT},\frac{\hbar}{(m_ek_BT)^{1/2}}\right) \tag{16}$$

where $\hbar=h/2\pi$ is the reduced Planck constant, ω is the laser frequency, and ω_p is the plasma frequency defined by

$$\omega_p=\sqrt{\frac{n_ee^2}{m_e\epsilon_0}} \tag{17}$$

where ϵ_0 is the electrical permittivity of free space.

2.4 Optical Properties. A critical task is to determine the laser source term in Eq. (1). A general expression for laser intensity (W/cm^2) I inside the bulk material for both nonlinear and linear absorptions is [21,22]

$$I(t,z)=\frac{2}{\sqrt{\pi/\ln 2}}\frac{J}{t_p}[1-R(t)]\exp\left[-(4\ln 2)\left(\frac{t}{t_p}\right)^2-\int_0^z\alpha(t,z)dz\right] \tag{18}$$

where J is the laser fluence in J/cm^2, t_p is the pulse duration, R is the reflectivity, and $\alpha(t,z)$ is the absorption coefficient. If the absorption coefficient is assumed to be a constant, using the definition that optical penetration depth $\delta=1/\alpha$ the laser source term (W/cm^{-3}) is simplified to the following expression commonly used in the existing model [5–8]:

$$S(t,z)=\frac{0.94J}{t_p\delta}[1-R(t)]\exp\left[-2.77\left(\frac{t}{t_p}\right)^2-\frac{z}{\delta}\right] \tag{19}$$

Rethfeld et al. have demonstrated that the ultrashort laser-metal interaction can be well described by laser-plasma interactions [1]. According to the Drude model for free electrons ϵ the electrical permittivity (dielectric function) of metals modeled as a plasma, is expressed as [23]

$$\mathbf{c}(t,z)=\epsilon_1(t,z)+i\epsilon_2(t,z)=1+\left(\frac{n_ee^2}{m_e\epsilon_0}\right)\left(\frac{-\tau_e^2(t,z)+i\tau_e(t,z)/\omega}{1+\omega^2\tau_e^2(t,z)}\right)$$
$$=1+\omega_p^2\left(\frac{-\tau_e^2(t,z)+i\tau_e(t,z)/\omega}{1+\omega^2\tau_e^2(t,z)}\right) \tag{20}$$

Equation (20) shows how the plasma frequency in Eq. (17) is defined.

The relationship between the complex refractive index $\mathbf{f}$ and the complex electrical permittivity is given by

$$\left(\frac{\mathbf{c}}{\mathbf{v}}\right)=\mathbf{f}=(f_1+if_2)=\sqrt{\boldsymbol{\epsilon}}=\sqrt{\epsilon_1+i\epsilon_2} \tag{21}$$

where $\mathbf{c}$ is the velocity of light in vacuum, $\mathbf{v}$ is the velocity of light in the material, f_1 is the normal refractive index, and f_2 is the extinction coefficient. Thus, the f_1 and f_2 functions can be derived as

$$f_1(t,z)=\sqrt{\frac{\epsilon_1(t,z)+\sqrt{\epsilon_1^2(t,z)+\epsilon_2^2(t,z)}}{2}},$$
$$f_2(t,z)=\sqrt{\frac{-\epsilon_1(t,z)+\sqrt{\epsilon_1^2(t,z)+\epsilon_2^2(t,z)}}{2}} \tag{22}$$

The reflectivity and the absorption coefficient of the metal are determined by the following Fresnel expression:

$$R(t)=\frac{[f_1(t,0)-1]^2+f_2^2(t,0)}{[f_1(t,0)+1]^2+f_2^2(t,0)},\quad \alpha(t,z)=\frac{2\omega f_2(t,z)}{c}=\frac{4\pi f_2(t,z)}{\lambda} \tag{23}$$

where λ is the wavelength of the laser.

However, the Drude model for metals, Eq. (20), does not consider the interband transition and the Fermi distribution. For gold, the d-band transition plays a critical role in the optical properties [4,14]. In d-band transition, electrons jump from the top of the d band to the unoccupied states near the Fermi level in the conduction band (p band). For noble metals like gold, the contribution of interband absorption to optical properties can be directly added to the Drude model, Eq. (20), for electrical permittivity [25]. Experiments have shown that the transient reflectivity of gold films is directly related to the change in the occupation number of electrons near the Fermi energy [14]. The change in occupied state distributions near the Fermi level caused by electron heating is called the Fermi distribution smearing [14]. Eesley estimated the distribution of occupied electronic states near the Fermi energy by [14]

$$\rho_F=\frac{1}{1+\exp\{[h\nu-(\varepsilon_F-\varepsilon_d)]/k_BT_e\}} \tag{24}$$

where ν is the laser frequency; $(\varepsilon_F-\varepsilon_d)=2.38$ eV for gold [4] is the difference between the Fermi energy and the d-band energy ε_d. It is seen the absorption of photon energy $h\nu$ is directly affected by the d-band transition. The smearing of the electron distribution is given by

$$\Delta\rho_F=\rho_F(h\nu,T_e)-\rho_F(h\nu,T_0) \tag{25}$$

which is linearly proportional to the imaginary component of the electrical permittivity in Eq. (20) [4]

$$\frac{\Delta\epsilon_2}{\epsilon_2}=\frac{\Delta\rho_F}{\rho_F} \tag{26}$$

where T_0 is the room temperature [4]. After adding $\Delta\epsilon_2$ to ϵ_2 in Eq. (20), the reflectivity and the absorption coefficient with the consideration of d-band transition can be determined by Eq. (23).

2.5 Phonon Heat Capacity. The above discussion addresses the temperature dependent properties of electrons. Similarly, the phonon heat capacity in Eq. (2) is also temperature dependent which can be calculated by the well-known quantum treatment, the Debye model [24] in which the average kinetic energy of phonons $\langle\varepsilon_p\rangle$ is calculated by [24]

$$\langle\varepsilon_p\rangle=\int_0^{\nu_{\max}}\frac{6\pi h}{n_ac_s^3}\frac{\nu^3}{e^{h\nu/kT_l}-1}d\nu \tag{27}$$

where n_a is the phonon number density and $\nu_{\max}$ is the maximum frequency of phonons calculated by

$$\nu_{\max}=\left(\frac{3}{4\pi}\right)^{1/3}\frac{c_s}{a} \tag{28}$$

where a is the average interatomic spacing, $a=(V/N)^{1/3}=(n_a)^{-1/3}$. The molar heat capacity of phonons can be calculated by

$$C_l(T_l)=2n_a\left(\frac{\partial\langle\varepsilon_p\rangle}{\partial T_l}\right)_V \tag{29}$$

where N_A is the Avogadro constant. The factor of 2 appears in Eq. (29) is used to account for both the kinetic energy and potential energy that are statistically equal in an ideal-lattice metal.

The two equations Eqs. (1) and (2) are solved by a fully implicit schedule with iterations at each time step for temperature-dependent thermal properties until convergence is achieved. Different grid sizes and time step sizes are employed to assure the final results are consistent.

3 Results and Discussion

3.1 Heat Capacity. First, some general discussions are presented about the heat capacities of free electrons and phonons in certain temperature ranges. Figure 1(*a*) demonstrates the significant differences in average kinetic energy of free electrons between the quantum treatment using Eqs. (5)–(10) and the ideal gas approximation using Eq. (12) for gold. At 300 K, the average kinetic energies of free electrons predicted by the quantum treat-

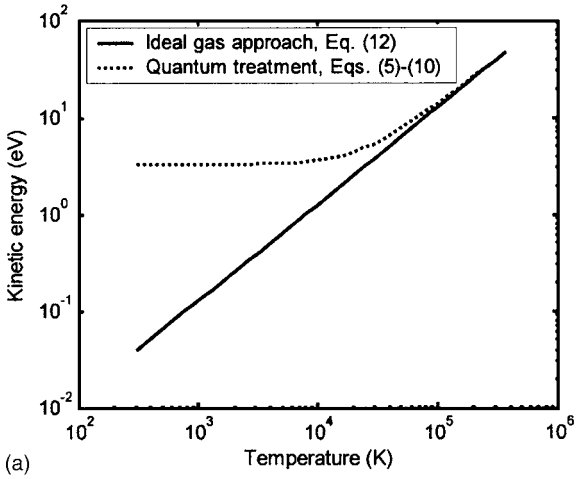

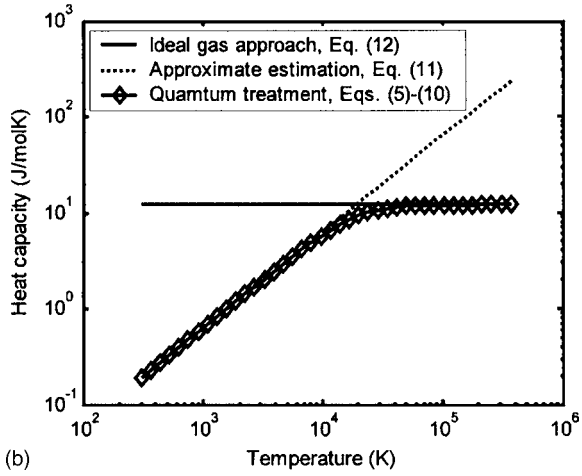

Fig. 1 The differences between different treatments for gold: (*a*) average free electron kinetic energy in electronvolts and (*b*) molar free electron specific heat

ment and classical approach are 3.3 and 0.039 eV, respectively, and they are different by about two orders of magnitude. It is seen only at temperatures much higher than the Fermi temperature (5.9×10^4 K for gold), the classical approach of Eq. (12) is valid. Figure 1(*b*) shows the significant differences between the ideal gas approach using Eq. (12), the approximation using Eq. (11), and the quantum treatment using Eqs. (5)–(10) for electron specific heat per mole. Equation (11) for $T_e \ll T_F$ and Eq. (12) for $T_e \gg T_F$ have been discussed for femtosecond laser ablation of metals [26] and yet the full-run quantum using Eq. (5)–(10) was not used in their work. At temperatures much lower than the Fermi temperature, the results by quantum treatment overlap with the approximations using Eq. (11) that is widely employed in the two-temperature model [5–8]. This implies when $T_e \ll T_F$, Eqs. (5)–(10) can be simplified to Eq. (11). Figure 1 clearly shows the necessity of quantum treatment for free electrons in the ultrashort laser-metal interaction.

On the other hand, the variation of gold phonon heat capacity in [300 K, 1337.33 K] calculated by the Debye model is insignificant, as shown in Fig. 2. In [300 K, 1337.33 K] for gold phonons, the molar phonon heat capacity predicted by the quantum treatment (the Debye model) is similar to that predicted by the classical estimation (the Law of Dulong and Petit) that states the molar heat capacity of metals is about $3R_u$, where R_u is the universal gas constant [24]. In fact, this is expected as the Debye temperature (the quantum characteristic temperature of phonons) of gold is 165 K that is low as compared to the phonon temperature. Hence,

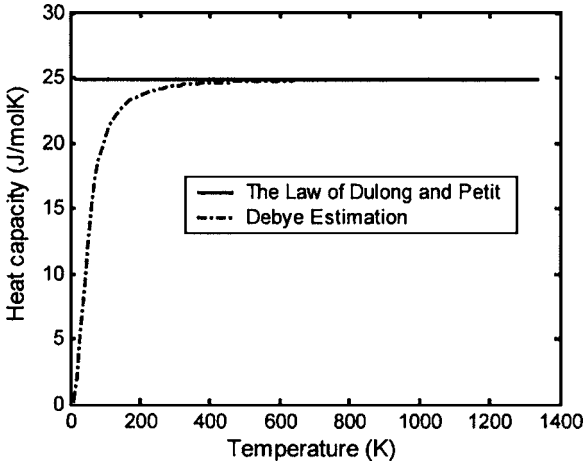

Fig. 2 Molar phonon specific heat predicted by different approaches

the lattice heat capacity of gold in the calculation can be reasonably considered as a constant. Note the gold heat capacity is the sum of the free electron heat capacity and phonon heat capacity.

3.2 Fermi Distribution Smearing. Figure 3 shows the smearing of electron distributions as a function of temperature at

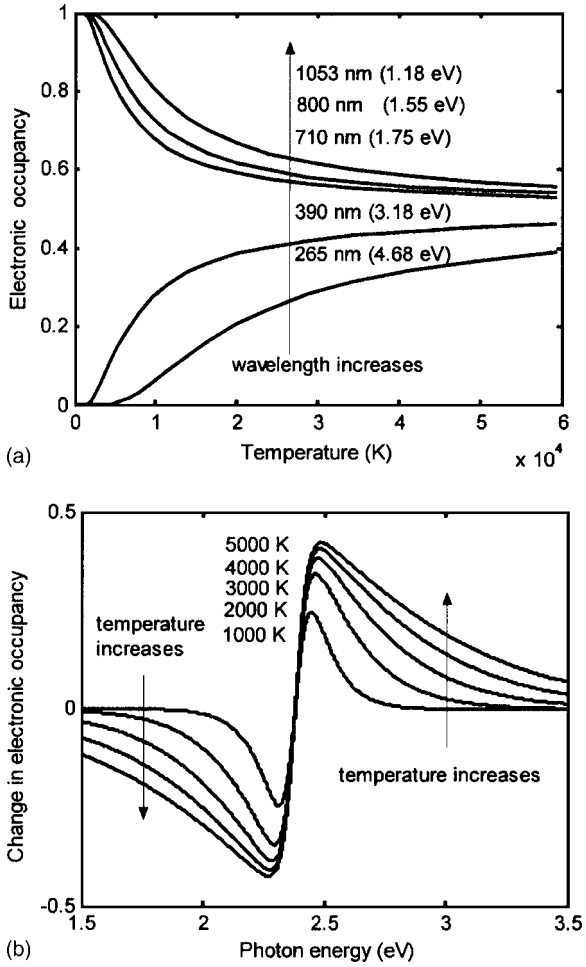

Fig. 3 Distribution of occupied electronic states near the Fermi energy: (*a*) electronic occupy and (*b*) change in electronic occupancy

different laser wavelengths in which T_0 is assumed to be 300 K. When the photon energy for a given wavelength, for example, 1.18 eV (1053 nm), is smaller than the difference between the Fermi energy and the *d*-band energy, $(\varepsilon_F - \varepsilon_d) = 2.38$ eV for gold, Fig. 3(*a*). This is true for all lasers with wavelengths above about 522 nm. On the other hand, when the photon energy, for example, 3.18 eV (390 nm), is higher than $(\varepsilon_F - \varepsilon_d)$, the Fermi distribution of occupied states increases in the heating process, which in turn increases the electron-phonon coupling. For both cases, as the electron temperature increases, the Fermi distribution of occupied states approaches a constant 0.5. Figure 3(*b*) shows the change in electronic occupancy as a function of laser wavelength. The merge of different curves near the 2.38 eV photon energy confirms the discussion given above.

3.3 Damage Threshold Fluence. This study calculates a 140 fs, 1053 nm laser heating of 200 nm gold film by using both the existing two-temperature model [5–8] and our proposed model. For this condition, the experimental threshold fluence is 0.43 ± 0.04 J/cm^2 [27]. By assuming the damage starts when the maximum lattice temperature reaches the melting temperature, 1337.33 K for gold, our model gives 0.45 J/cm^2 for the threshold fluence, while the existing two-temperature model gives 0.75 J/cm^2.

At 0.45 J/cm^2, the temperature distributions of the electrons and the lattice predicted by the proposed model are shown in Fig. 4. As shown in the figure, the electron temperature can reach as high as 2.12×10^4 K which is well beyond the electron temperature range $(0 < T_e < 0.1\ T_F)$. Thus, in the existing model [5–8], the simplified estimations of electron heat capacity, electron heat conductivity, electron relaxation time, and reflectivity, as mentioned earlier, may not be adequate.

3.4 Comparisons Between the Existing Model and the Proposed Model. At 0.05 J/cm^2, a low laser fluence with respect to the threshold fluence, the calculated results for a 200 nm gold film by the existing model and the proposed model are very similar in both the electron temperatures and phonon temperatures, as shown in Fig. 5. It is seen the highest electron temperature 3347 K predicted by the proposed model, is within the low electron temperature range for free electrons. In low fluences, the similarities between results from the existing model and the proposed models are expected, because the full-run quantum treatment can be simplified to the existing model for low electron temperatures. The slight difference between the predictions of the two models is mainly caused by the different treatments in reflectivity. In the existing model, reflectivity estimation $\Delta T_e/(\Delta T_e)_{\max} \cong \Delta R/(\Delta R)_{\max}$ is limited to $300\ \text{K} < T_e < 700$ K that is much lower than the highest electron temperature 3347 K, under 0.05 J/cm^2.

On the other hand, at 0.2 J/cm^2, a fluence comparable to the threshold fluence, significant differences between the two models are observed in Fig. 6. This confirms the need to estimate the thermal and optical properties with quantum treatments for the ultrashort laser heating of metals at fluences comparable to the threshold fluence.

3.5 Effect of Pulse Duration. This study also investigates the effect of pulse duration on the damage threshold. As shown in Fig. 7, the proposed model significantly increases the prediction accuracy of the damage thresholds compared with the existing model. At the wavelength of 1053 nm, the damage thresholds of 200 nm film predicted by the proposed model are almost independent of the pulse duration in 140 fs–100 ps, which is confirmed by the experimental data [27]. As shown in Fig. 7, the predicted trend of the damage thresholds by our proposed model can be roughly divided into two ranges: 140 fs–10 ps and 10 ps–100 ps with the turning point around 10 ps. It is expected for the threshold fluence to increase with the increase of the pulse duration in 10 ps–100 ps. However, the properties of the 200 nm thin film are quite different

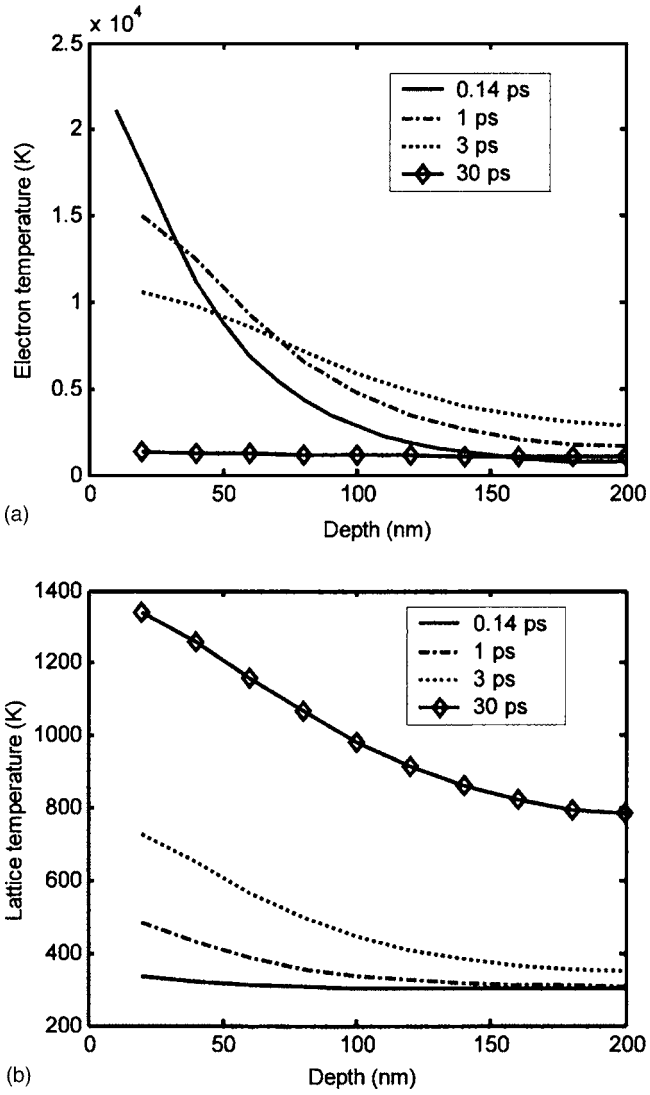

Fig. 4 (*a*) electron temperature distribution and (*b*) lattice temperature distribution at different times predicted by the proposed model for a 200 nm gold film irradiated by a 140 fs, 1053 nm pulse at 0.45 J/cm^2

with its bulk material when the thin film thickness is comparable to the optical penetration depth. In 140 fs–10 ps, for the 200 nm thin film, the shorter pulse duration leads to(1) the higher electron temperature and hence higher heat conductivity, causing a more uniform temperature distribution in the thin film after the thermalization time at which the maximum lattice temperature is expected. This factor tends to increase the threshold fluence; and (2) the stronger transient changes in the reflectivity of gold film during the 1053 nm pulse irradiation that tends to decrease threshold fluence [16]. Hence, roughly speaking, these two factors balance each other, which makes the threshold fluence in 140 fs–10 ps almost independent of pulse duration.

4 Conclusions

This study introduces full-run quantum treatments to the two-temperature model for several critical optical and thermal properties, including the electron heat capacity, electron relaxation time, electron conductivity, reflectivity and absorption coefficient. The proposed model releases the low temperature limitation of the existing estimations on optical and thermal properties and effectively extends the application range to high laser fluences. On the other hand, at low temperature ranges, the proposed full-run quan-

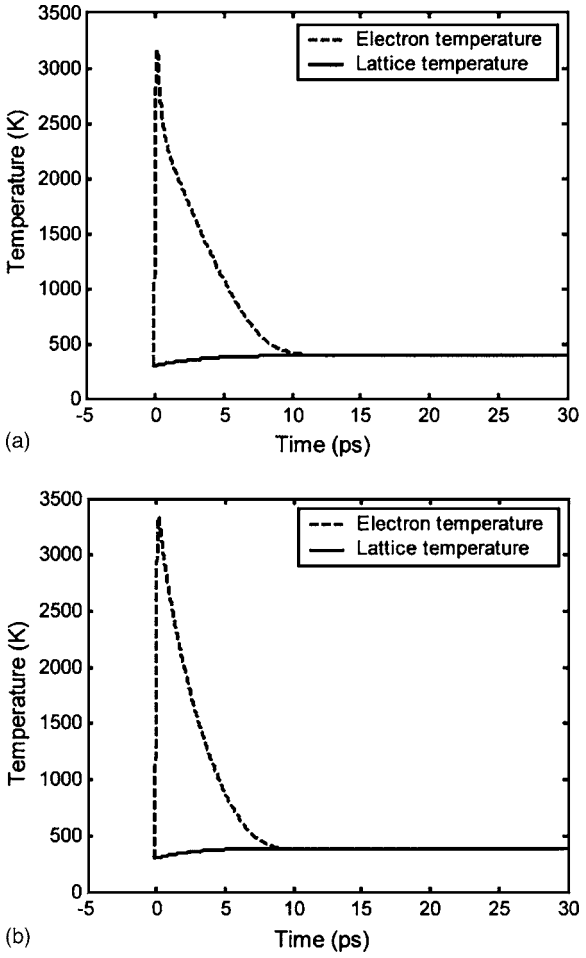

Fig. 5 Surface temperature as a function of time for 200 nm gold film irradiated by a 140 fs, 1053 nm pulse at 0.05 J/cm^2: (*a*) the existing model and (*b*) the proposed model

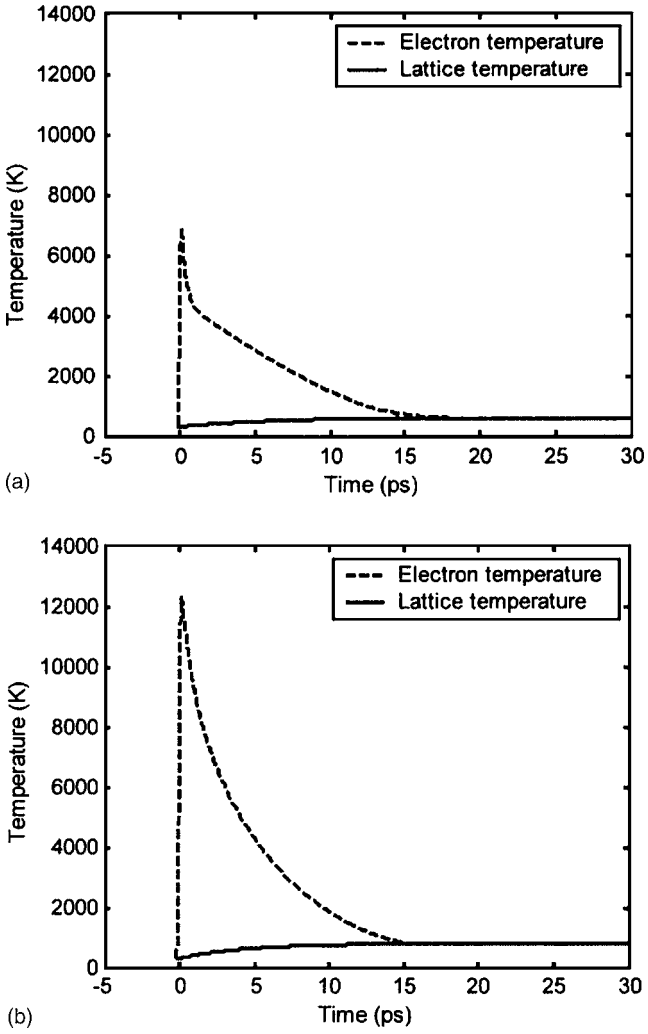

Fig. 6 Surface temperature as a function of time for 200 nm gold film irradiated by a 140 fs, 1053 nm pulse at 0.2 J/cm^2: (*a*) the existing model (*b*) the proposed model

tum treatments can be simplified to those employed by the existing two-temperature model, which is proved by either mathematical derivations or simulation results. The proposed model is employed to calculate the heating process of thin gold films until melting occurs, which is assumed to be the initiation of damage. The predicted damage threshold fluences for 200 nm gold film by the proposed model are in good agreement with published experimental data. The predicted damage thresholds of thin films are almost independent of pulse duration in the ultrashort ($<$10 ps pulse range, as confirmed by experiments.

Acknowledgment

This work was supported by the Air Force Research Laboratory under Contract No. FA8650-04-C-5704 and the National Science Foundation under Grant No. 0423233.

Nomenclature

a = average interatomic spacing
B = bulk modulus
b_{max} = maximum collision parameter in Eq. (15)
b_{min} = minimum collision parameter in Eq. (15)
c = speed of light in vacuum
$\mathbf{c}$ = velocity of light in vacuum
C_e = electron heat capacity
C_l = lattice heat capacity
c_s = speed of sound
e = electron charge

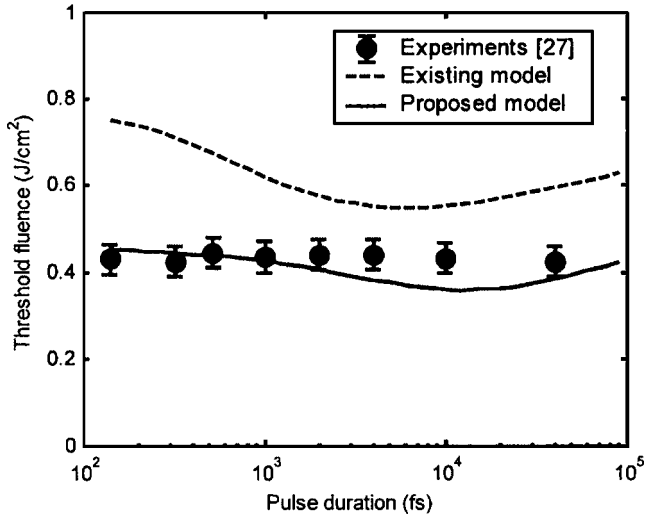

Fig. 7 Damage threshold fluences of 200 nm gold film processed by a 1053 nm laser at different pulse durations

k_B = Boltzmann constant
$\mathbf{f}$ = complex refractive index
f_1 = normal refractive index
f_2 = extinction coefficient
G = electron-lattice coupling factor
h = Planck constant
$\hbar$ = reduced Planck constant
I = laser intensity
J = laser fluence in J/cm^2
k_B = Boltzmann's constant
k_e = electron conductivity
k_{eq} = electron heat conductivity in the electron-phonon thermal equilibrium
m_e = nonrelativistic mass of a free electron
n_a = phonon number density
n_e = density of the free electrons
$\langle n_k \rangle$ = average number of electrons in energy state ε_k
N_A = Avogadro constant
N_e = Total number of free electrons
R = reflectivity
R_u = universal gas constant
S = laser source term
t = time
t_p = pulse duration
T_D = Debye temperature
T_e = electron temperature
T_F = Fermi temperature
T_l = lattice temperature
T_0 = room temperature
V = volume
v_e^2 = mean square of electron speed
v_s = sound speed in the metal
Z^* = ionization state

Greek Symbols

α = absorption coefficient
δ = optical penetration depth
$\boldsymbol{\epsilon}$ = complex dielectric function
ϵ_0 = electrical permittivity of free space
ϵ_1 = real part of the dielectric function
ϵ_2 = imaginary part of the dielectric function
$\langle \varepsilon \rangle$ = average electron kinetic energy
$\langle \varepsilon_p \rangle$ = average phonon kinetic energy
ε_d = d-band energy
ε_F = Fermi energy
ε_k = electron energy state
$\ln \Lambda$ = Coulomb logarithm in Eq. (14)
γ = electron heat capacity constant in Eq. (11)
λ = wavelength of the laser
μ = chemical potential
ν = laser frequency
ν_{max} = maximum frequency of phonons
ρ = density of states
ρ_F = distribution of occupied electronic states
ρ_m = density
τ = electron relaxation time
ω = laser frequency
ω_p = plasma frequency

References

[1] Rethfeld, B., Kaiser, A., Vicanek, M., and Simon, G., 2002, "Ultrafast Dynamics of Nonequilibrium Electrons in Metals under Femtosecond Laser Irradiation," Phys. Rev. B, **65**, pp. 214303–214313.
[2] Del Fatti, N., Voisin, C., Achermann, M., Tzortzakis, S., Christofilos, D., and Vallee, F., 2000, "Nonequilibrium Electron Dynamics in Noble Metals," Phys. Rev. B, **61**, pp. 16956–16966.
[3] Fujimoto, J. G., Liu, J. M., Ippen, E. P., and Bloembergen, N., 1984, "Femtosecond Laser Interaction with Metallic Tungsten and Nonequilibrium Electron and Lattice Temperatures," Phys. Rev. Lett., **53**, pp. 1837–1840.
[4] Schoenlein, R. W., Lin, W. Z., Fujimoto, J. G., and Eesley, G. L., 1987, "Femtosecond Studies of Nonequilibrium Electronic Processes in Metals," Phys. Rev. Lett., **58**, pp. 1680–1683.
[5] Qiu, T. Q., and Tien, C. L., 1992, "Short-Pulse Laser Heating on Metals," Int. J. Heat Mass Transfer, **35**, pp. 719–726.
[6] Qiu, T. Q., and Tien, C. L., 1993, "Heat Transfer Mechanisms during Short-Pulse Laser Heating of Metals," ASME J. Heat Transfer, **115**, pp. 835–841.
[7] Qiu, T. Q., and Tien, C. L., 1994, "Femtosecond Laser Heating of Multi-Layer Metals-I Analysis," Int. J. Heat Mass Transfer, **37**, pp. 2789–2797.
[8] Qiu, T. Q., Juhasz, T., Suarez, C., Bron, W. E., and Tien, C. L., 1994, "Femtosecond Laser Heating of Multi-Layer Metals-II Experiments," Int. J. Heat Mass Transfer, **37**, pp. 2799–2808.
[9] Tzou, D. Y., Chen, J. K., and Beraun, J. E., 2002, "Hot-Electron Blast Induced by Ultrashort-Pulsed Lasers in Layered Media," Int. J. Heat Mass Transfer, **45**, pp. 3369–3382.
[10] Elsayed-Ali, H. E., Norris, T. B., Pessot, M. A., and Mourou, G. A., 1987, "Time-Resolved Observation of Electron-Phonon Relaxation in Copper," Phys. Rev. Lett. **58**, pp. 1212–1215.
[11] Schoenlein, R. W., Lin, W. Z., Fujimoto, J. G., and Eesley, G. L., 1987, "Femtosecond Studies of Nonequilibrium Electronic Processes in Metals," Phys. Rev. Lett., **58**, pp. 1680–1683.
[12] Hertel, T., Knoesel, E., Wolf, M., and Ertl, G., 1996, "Ultrafast Electron Dynamics at Cu(111): Response of an Electron Gas to Optical Excitation," Phys. Rev. Lett., **76**, pp. 535–538.
[13] Brorson, S. D., Kazeroonian, A., Moodera, J. S., Face, D. W., Cheng, T. K., Ippen, E. P., Dresselhaus, M. S., and Dresselhaus, G., 1990, "Femtosecond Room-Temperature Measurement of the Electron-Phonon Coupling Constant Gamma in Metallic Superconductors," Phys. Rev. Lett., **64**, pp. 2172–2175.
[14] Eesley, G. L., 1986, "Generation of Nonequilibrium Electron and Lattice Temperatures in Copper by Picosecond Laser Pulses," Phys. Rev. B, **33**, pp. 2144–2151.
[15] Anisimov, S. I., Kapeliovich, B. L., and Perel'man, T. L., 1974, "Electron Emission from Metal Surfaces Exposed to Ultrashort Laser Pulses," Sov. Phys. JETP, **39**, pp. 375–377.
[16] Wellershoff, S., Hohlfeld, J., Güdde, J., Matthias, E., 1999, "The Role of Electron-Phonon Coupling in Femtosecond Laser Damage of Metals," Appl. Phys. A: Mater. Sci. Process. **69**(Suppl.), pp. 99–107.
[17] Ashcroft, N. W., and Mermin, N. D., 1976, *Solid State Physics*, Holt, Rinehart, and Winston, New York.
[18] Kittel, C., 1986, *Introduction to Solid State Physics*, J Wiley, NY.
[19] Gamaly, E. G., Rode, A. V., Luther-Davies, B., and Tikhonchuk, V. T., 2002, "Ablation of Solids by Femtosecond Lasers: Ablation Mechanism and Ablation Thresholds for Metals and Dielectrics," Phys. Plasmas, **9**, pp. 949–957.
[20] Lee, Y. T., and More, R. M., 1984, "An Electron Conductivity Model for Dense Plasma," Phys. Fluids, **27**(5), pp. 1273–1286.
[21] Jiang, L., and Tsai, H. L., 2004, "Prediction of Crater Shape in Femtosecond Laser Ablation of Dielectrics," J. Phys. D **37**, pp. 1492–1496.
[22] Jiang, L., and Tsai, H. L., 2005, "Energy Transport and Material Removal during Femtosecond Laser Ablation of Wide Bandgap Materials," Int. J. Heat Mass Transfer, **48** (3–4), pp. 487–499.
[23] Fox, M., 2001, *Optical Properties of Solids*, Oxford University Press, Oxford.
[24] Baierlein, R., 1999, *Thermal Physics*, Cambridge University Press, New York.
[25] Palpant, B., Prével, B., Lermé, J., Cottancin, E., and Pellarin, M., 1998, "Optical Properties of Gold Clusters in the Size Range 2-4 nm," Phys. Rev. B, **57**, pp. 1963–1970.
[26] Nolte, S., Momma, C., Jacobs, H., Tunnermann, A., Chichkov, B. N., Wellegehausen, B., and Welling, H., 1997, "Ablation of Metals by Ultrashort Laser Pulses," J. Opt. Soc. Am. B **14**, pp. 2716–2722.
[27] Stuart, B. C., Feit, M. D., Herman, S., Rubenchik, A. M., Shore, B. W., and Perry, M. D., 1996, "Optical Ablation by High-Power Short-Pulse Lasers," J. Opt. Soc. Am. B, **13**, pp. 459–468.